Application of catastrophe theory to multicolor-laser-field-assisted scattering

Dino Habibović[1†], Thomas Rook[2†], Dejan B. Milošević[1,3*†]

[1]Faculty of Science, University of Sarajevo, Zmaja od Bosne 35, Sarajevo, 71000, Bosnia and Herzegovina.
[2]Department of Physics, University of Oxford, Clarendon Laboratory, Parks Road, Oxford, OX1 3PU, United Kingdom.
[3]Academy of Sciences and Arts of Bosnia and Herzegovina, Bistrik 7, Sarajevo, 71000, Bosnia and Herzegovina.

*Corresponding author(s). E-mail(s): milo@bih.net.ba;
Contributing authors: dhfizika1@gmail.com;
thomas.rook@physics.ox.ac.uk;
†These authors contributed equally to this work.

Abstract

Strong-field processes are highly nonlinear, often involving the absorption of thousands of photons, which can lead to the emission of high harmonics in the soft X-ray region or the production of high-energy electrons carrying information about the target. The transition amplitudes of these processes are typically expressed as integrals over time, where the phase of the subintegral function is determined by a strong-field-dependent action. This structure allows the use of asymptotic methods for integrals and forms the basis of quantum-orbit theory, which provided valuable physical insight and led to new discoveries. Here, we show how highly nonlinear laser-assisted processes can be systematically investigated using the powerful mathematical apparatus of catastrophe theory. Using laser-assisted scattering as an example, we demonstrate how catastrophe theory can identify critical values of control parameters for which qualitative changes occur in the spectral response, i.e., where the catastrophes appear. We illustrate this with the fold, cusp, swallowtail, and wigwam catastrophes.

Keywords: strong-field physics, laser-assisted scattering, catastrophe theory

Introduction

Strong-field physics and attoscience are areas of modern physics which have developed after the discovery of lasers capable of delivering strong and ultrashort pulses [1–5]. Laser-assisted processes can occur in the absence of a laser field, but, when a laser field is applied, new characteristics of these processes emerge [6, 7]. Examples are laser-assisted electron-atom scattering [8, 9], X-ray–atom scattering in the presence of a laser field [10, 11], and laser-assisted electron-ion radiative recombination [12, 13]. On the other hand, laser-induced processes can only happen in the presence of the laser field [14–21]. Examples are above-threshold ionization and high-order harmonic generation in which the emitted coherent soft X-rays led to important applications [3, 5]. Despite the extensive study of strong-field processes, the systematic exploration of their critical structures from geometric and topological point of view has not been undertaken until now. In this work, we apply catastrophe theory to tackle this issue, providing a toolset for the analysis and interpretation of the critical structures in strong-field processes. We will limit our analysis to laser-assisted processes.

From the theoretical point of view, the fact that the laser field is strong has prevented application of standard perturbative quantum-mechanical methods for analysis of these processes. *Ab-initio* methods like numerical solutions of the time-dependent Schrödinger equation [22] are time-consuming and they do not provide adequate physical explanations. Fortunately, the fact that the laser field is strong can be used to develop nonperturbative theories such as the strong-field approximation (SFA; see, for example, the review articles [6, 14, 19]). For laser-assisted scattering (LAS) an analog of the SFA theory was given in [23].

Laser-assisted electron-atom scattering, or multiphoton free-free collision, is a process in which L photons ($L = 0, \pm1, \pm2, \pm3, \ldots$) are exchanged with the laser field during electron-atom scattering. The differential cross section (DCS) of this process as a function of the observed final electron energy exhibits peaks which are shifted by the energy $L\hbar\omega$ ($\hbar\omega$ is the laser photon energy) with respect to the elastic scattering peak ($L = 0$). LAS was observed almost 50 years ago [8], even before the famous above-threshold ionization experiment by Agostini et al. [24] and high-order harmonic generation experiment by L'Huillier et al. [25], which were seminal for strong-field physics and attoscience [3–5]. For earlier reviews about the LAS process, see [26] (for experiment) and [9] (for theory). For a review of more recent experimental results see [27].

In this work, we apply catastrophe theory to study laser-assisted processes. Although catastrophe theory has been widely used in the analysis of wavefront singularities and other optical phenomena, its application in strong-field physics has been less thoroughly explored. Here, we demonstrate that catastrophe theory provides a powerful and systematic framework for predicting the emergence of critical points, bifurcations, and discontinuities in laser-assisted dynamics. Historically, Thom [28] classified seven elementary catastrophes, which serve as universal models for abrupt transitions across diverse scientific fields [29]. Arnold has extended Thom's elementary catastrophes and introduced ADE classification [30, 31]. Berry applied these concepts to singularities in wavefronts [32, 33]. More information about catastrophe theory can

be found in [34–36]. In the framework of strong-field physics, we mention that the cut-off in the energy spectrum of high-order harmonics has been considered as a caustic, which is related to the fold catastrophe [37–43]. For catastrophes in the context of ionization of atoms and molecules, see [44–53]. Caustic structures in Compton scattering were considered in [54, 55].

Methods

Laser-assisted scattering

We investigate the LAS process in a multicolor linearly polarized field [56] for which the scattering amplitude contains the laser-dependent factor $\int dt e^{iS_L(t)}$, where $S_L(t)$ is the action and the integration is over the scattering time t. This integral can be solved numerically (we will refer to this as the exact result), or approximately using the stationary-phase (SP) method in which case the LAS amplitude is expressed as a coherent sum of the partial amplitudes (in the fashion of Feynman's path integral [57, 58]). The sum is over particular solutions of the SP equation $S'_L(t) = 0$. More precisely, the above integral for a strong field can be approximated using asymptotic analysis of integrals [59]. This is done by expanding the action in its Taylor series about the stationary point t_s: $S_L(t) = S_L(t_s)+S''_L(t_s)(t-t_s)^2/2!+S'''_L(t_s)(t-t_s)^3/3!+\cdots$. If, at some critical value of the external parameters, two stationary points t_1 and t_2 coincide, giving a single stationary point $t_c = t_1 = t_2$ at which $S''_L(t_c) = 0$, we have to apply a uniform approximation containing Airy functions [59–61]. If three stationary points coalesce, we also have $S'''_L(t_s) = 0$, the fourth-order term of the above series should be considered and the result is expressed in terms of the Pearcey integral. For the four coalescing stationary points one should use the so-called swallowtail integral [60, 61], and so on. Therefore, depending on the external parameters, various critical situations can appear. In particular, as parameter values pass through the so-called bifurcation set, defined through the above degenerate critical points, qualitative changes happen. A bifurcation set is the locus in the control parameter space where the system's equilibrium structure changes. Such "boundaries" in parameter space separate regions of different system behaviors (cf. figures in the paper and Supplementary Notes 1 and 2). In the present paper, we pioneer the application of catastrophe theory to the laser-assisted scattering process. This approach provides a systematic framework for identifying and classifying critical points and bifurcation structures that shape the scattering dynamics. Moreover, the methodology (after a generalization to complex-valued saddle points) may provide a useful framework for the analysis of laser-induced processes. The applicability of catastrophe theory to processes involving strong-field tunnelling remains an open question, and it may offer new perspectives on strong-field phenomena where complex bifurcation patterns play an important role.

For a T-periodic laser field with the fundamental frequency $\omega = 2\pi/T$, the DCS for the electron scattering on the potential $V(\mathbf{r})$ is defined by [7, 9, 62] (in atomic units) $d\sigma_{\rm fi}/d\Omega = (2\pi)^4 k_{\rm f}|T_{\rm fi}(L)|^2/k_{\rm i}$, where $\mathbf{k}_{\rm i}$ ($\mathbf{k}_{\rm f}$) is the initial (final) electron momentum, and $T_{\rm fi}(L)$ is the T-matrix element for scattering with exchange of L photons. The energy-conservation condition is $E_{\rm f} = E_{\rm i} + L\omega$, $E_j = k_j^2/2$, $k_j = |\mathbf{k}_j|$, $j = {\rm i}, {\rm f}$. In the

first Born approximation it is [62]

$$T_{\rm fi}(L) = V_{\mathbf{q}} \int_0^T dt \mathrm{e}^{\mathrm{i}S_L(t)},\ S_L(t) = L\omega t + \mathbf{q}\cdot\boldsymbol{\alpha}(t), \tag{1}$$

where $V_{\mathbf{q}} = \int d^3\mathbf{r} V(\mathbf{r})\mathrm{e}^{-\mathrm{i}\mathbf{q}\cdot\mathbf{r}}/T$, $\mathbf{q} = \mathbf{k}_{\rm f} - \mathbf{k}_{\rm i}$, $\boldsymbol{\alpha}(t) = \int^t d\tau \mathbf{A}(\tau)$, and $\mathbf{A}(t) = -\int^t d\tau \mathbf{E}(\tau)$, with $\mathbf{E}(t)$ the electric-field vector. Using the condition that the action is stationary, $dS_L(t)/dt = 0$, we obtain the SP equation $[\mathbf{k}_{\rm i} + \mathbf{A}(t)]^2/2 = [\mathbf{k}_{\rm f} + \mathbf{A}(t)]^2/2$. Neglecting higher order than quadratic terms in the Taylor series expansion of $S_L(t)$, the SP approximation gives [63]

$$T_{\rm fi}^{\rm SP}(L) = V_{\mathbf{q}} \sum_{t_s} \sqrt{\frac{2\pi}{|S_L''(t_s)|}} \mathrm{e}^{\mathrm{i}S_L(t_s) + \mathrm{i}\,\mathrm{sign}\left[S_L''(t_s)\right]\pi/4}, \tag{2}$$

where the sum is over all stationary points t_s which are solutions of the SP equations.

Catastrophe theory

The SP approximation (2) cannot be applied if we have critical coalescing SP points in which higher-order derivatives of the action are zero. These critical points can be identified using catastrophe theory. For this purpose we replace $T_{\rm fi}(L)$ by the catastrophe integral [32, 33] $\mathcal{T}_{\rm fi}(\mathcal{C}) = V_{\mathbf{q}} \int_0^T dt \mathrm{e}^{\mathrm{i}\mathcal{S}(t;\mathcal{C})}$, where $\mathcal{S}(t;\mathcal{C})$ in our case is equal to $S_L(t)$ (and therefore has the same SP structure) and $\mathcal{C} = \{c_1, c_2, \ldots, c_m\}$ denotes the set of control parameters that influence the system (m is the control dimension or codimension). Our integration variable t is called the behavior or state variable (in our case the behavior dimension or the corank is one). Depending on the values of control parameters, various catastrophes may appear. For example, if the action $\mathcal{S}(t;\mathcal{C})$ is quadratic in t, the problem is structurally stable leading to the so-called zero unfolding. This corresponds to the SP method. An action that is cubic in t can always be written in the form $\mathcal{S}(t;c_1) = t^3/3 + c_1 t$. This case corresponds to the fold catastrophe, denoted by Arnold's symbol A_2 (see Table 1 in [33]), and it is related to the uniform approximation for two coalescing stationary points. In particular, the fold occurs when $\partial\mathcal{S}(t;c_1)/\partial t = 0$ and $\partial^2\mathcal{S}(t;c_1)/\partial t^2 = 0$, i.e., $t^2 + c_1 = 0$ (this curve is called equilibrium surface) and $2t = 0$, so that $t = \pm\sqrt{c_1} = 0$, and the bifurcation set is the point $c_1 = 0$. This set divides the control space into regions $c_1 > 0$ (here the equation $t^2 + c_1 = 0$ has no real solutions), and $c_1 < 0$, where there are two critical points which merge into a point of inflection for $c_1 = 0$. If the action $\mathcal{S}(t;\mathcal{C})$ is a fourth-order polynomial in t, it can be written as $\mathcal{S}(t;c_1,c_2) = t^4/4 + c_2 t^2/2 + c_1 t$ [33]. In this case, a fold occurs when both the first and the second derivatives vanish, leading to the system of equations $t^3 + c_2 t + c_1 = 0$ and $3t^2 + c_2 = 0$, which solution is the equation $27c_1^2 + 4c_2^3 = 0$ that describes a semicubical parabola. The cusp occurs when the first, second, and third derivatives are zero, that is, for $c_1 = c_2 = t = 0$. In this case, the equation $\partial\mathcal{S}(t;\mathcal{C})/\partial t = 0$ has a triple root (this catastrophe is denoted by Arnold's symbol A_3) and it is thus related to the Pearcey integral. Geometrically, a cusp forms where two folds meet and end – the tip of the cusp is the point where the folds come together and disappear [33]. The swallowtail catastrophe corresponds to the

polynomial $\mathcal{S}(t; c_1, c_2, c_3) = t^5/5 + c_3 t^3/3 + c_2 t^2/2 + c_1 t$ and its equilibrium hypersurface, for which $\partial\mathcal{S}(t; c_1, c_2, c_3)/\partial t = 0$, is given by the equation $t^4 + c_3 t^2 + c_2 t + c_1 = 0$. The corresponding singularity set is the subset of this hypersurface for which the equation $\partial^2\mathcal{S}(t; c_1, c_2, c_3)/\partial t^2 = 0$, i.e., $4t^3 + 2c_3 t + c_2 = 0$, also holds. The bifurcation set for the swallowtail catastrophe is a surface in the three-dimensional control space, which is obtained by eliminating the state variable t from the system of equations $t^4 + c_3 t^2 + c_2 t + c_1 = 0$ and $4t^3 + 2c_3 t + c_2 = 0$. The swallowtail catastrophe is denoted by Arnold's symbol A_4 and is characterized by the four coalescing critical points. Examples of fold, cusp, and swallowtail catastrophes for our LAS process are illustrated in figures in the paper. Finally, the last of the Thom's cuspoids, the butterfly catastrophe, corresponds to the polynomial $\mathcal{S}(t; c_1, c_2, c_3, c_4) = t^6/6 + c_4 t^4/4 + c_3 t^3/3 + c_2 t^2/2 + c_1 t$. It is denoted by Arnold's symbol A_5 and has five coalescing critical points. The Arnold's A_6 catastrophe, which is beyond Thom's elementary catastrophes, corresponds to the seventh order polynomial and is characterized by six coalescing stationary points. We will present a cross-section of it at the end of section Results (see also Supplementary Note 2). The structurally stable unfolding of the A_n singularity (for A_3 this is the cusp) may only be represented in $(n-1)$-control variables and one behavior variable. This makes it difficult to directly visualise catastrophes with codimension higher than that of the cusp. However, we can remedy this by studying cross-sections of the parameter space or by considering stratifications of catastrophes.

If the laser-field-driven electron in LAS process returns to the atom and rescatters off it, the corresponding T-matrix element can be expressed as the double integral over the first scattering time and the second scattering time (or over the travel time between two scatterings) [62]. This problem can also be treated using catastrophe theory. However, in this case the behavior dimension (corank) is two and we have the so-called umbilic catastrophes. Thom's elementary umbilics are hyperbolic and elliptic umbilics, which have codimension three and are denoted by Arnold's symbol $D_4^{\pm}$, and parabolic umbilic with codimension four and denoted by the symbol D_5.

Results

LAS by multicolor fields

We apply the catastrophe-theory framework to potential scattering in an n-color linearly polarized laser field [56], demonstrating how this methodology opens a pathway for analyzing and predicting the behavior of the laser-assisted scattering amplitudes across a broad parameter space. We suppose that the frequencies of our n-color field are commensurate. The case of incommensurable frequencies, i.e., irrational ratios between the driving laser field frequencies, fundamentally changes the dynamics of the scattering process and we will not consider it here (for bichromatic fields this quasiperiodic case can be treated using 2D-time formalism with a Floquet representation; see, for example, [64, 65]). We use the electric-field vector $\mathbf{E}(t) = E(t)\hat{\mathbf{e}}$ ($\hat{\mathbf{e}}$ - the polarization direction), $E(t) = E_0 \sum_{j=1}^{n} \xi_j \sin(j\omega t + \phi_j)$ (E_0 - the electric-field amplitude; ξ_j and ϕ_j - the relative amplitudes and phases, respectively). Denoting $A(t) = A_0 \sum_{j=1}^{n} a_j \cos(j\omega t + \phi_j)$, $A_0 = E_0/\omega$, $a_j = \xi_j/j$, $\varphi = \omega t$, the SP equation

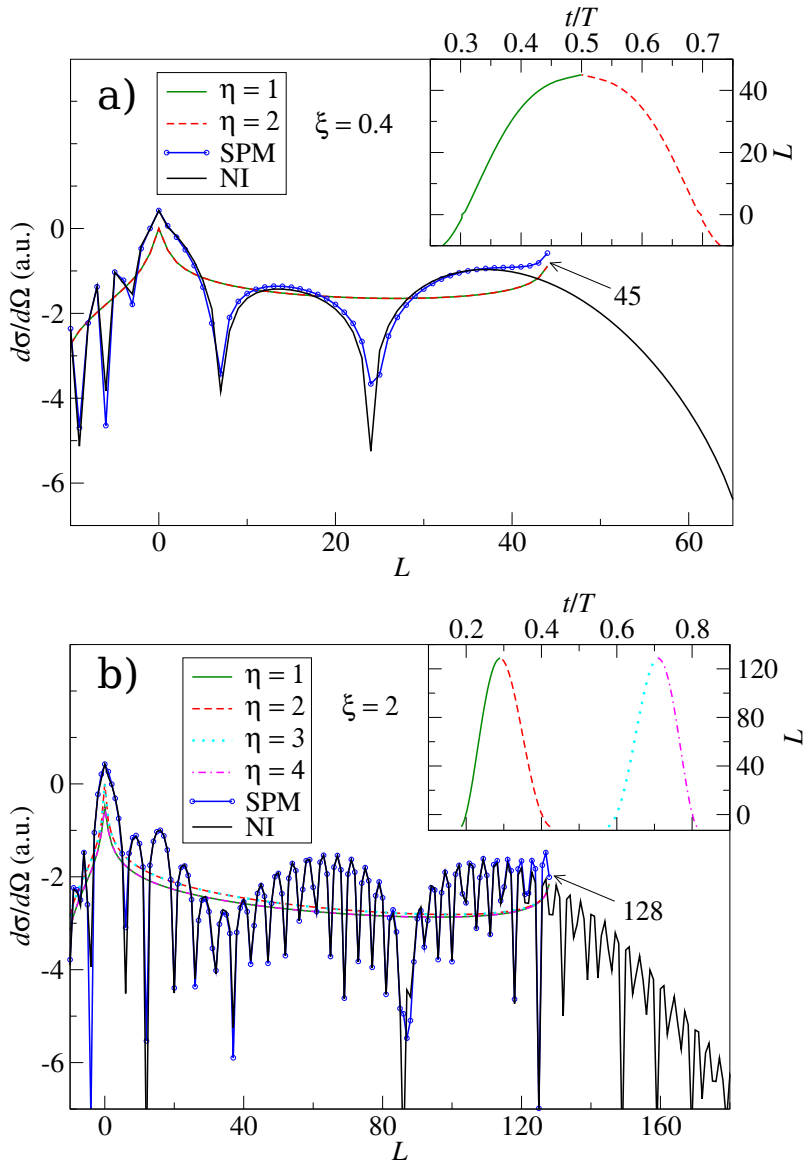

Fig. 1 Differential cross section for laser-assisted scattering.
The partial contributions of the SP solutions to the DCS for electron scattering on the He atom in the presence of the ω–2ω field as a function of the number of exchanged photons L. The ratio of the electric-field amplitudes is: a) $\xi = 0.4$ and b) $\xi = 2$, as denoted in the panels. The laser intensity, relative phase, and wavelength are $E_0^2 = 3 \times 10^{14}$ W cm^{-2}, $\phi = 0$, and 1000 nm, respectively. The initial electron kinetic energy is 0.5 a.u. and the electron momenta are in the polarization direction. We also present the coherent sum of the partial contributions (blue line, circles) and the exact result (black solid line). The insets show the SP solutions.

becomes

$$F(\varphi) = a_0 + \sum_{j=1}^{n} a_j \cos(j\varphi + \phi_j) = 0,\ a_0 = \frac{L\omega}{A_0 \mathbf{q}\cdot\hat{\mathbf{e}}}. \tag{3}$$

Here $F(\varphi)$ is a trigonometric polynomial of the nth order with real coefficients, so that (3) has $2n$ complex zeros φ_k, $0 \le \mathrm{Re}\,\varphi_k < 2\pi$, $k = 1, \ldots, 2n$ [59, 66]. Therefore, the maximum number of real solutions φ_k is equal to $2n$. For some field configurations the dependence of the number of real solutions on the field parameters and the initial and final electron energy can be found analytically, but, in general, in order to find this number we should use catastrophe theory.

We first investigate the case of the ω–2ω driving field with $\xi_1 = 1$, $\xi_2 = \xi$, $\phi_1 = \phi_2 = 0$. In this case, the SP equation becomes $\xi\cos^2\varphi + \cos\varphi + a_0 - \xi/2 = 0$, where $-1 \le \cos\varphi \le 1$, and, for the solutions to be real, the discriminant $D = 1 - 4\xi(a_0 - \xi/2)$ has to be nonnegative. This leads to the condition $a_0 \le 1/(4\xi) + \xi/2$. Let us assume that the intensity of the ω component is $E_0^2 = 3\times 10^{14}$ W cm^{-2}, while the corresponding wavelength is 1000 nm. For example, for the electron momenta in the polarization direction, $E_\mathrm{i} = 0.5$ a.u., and $E_\mathrm{f} = 2$ a.u., it is $a_0 = 0.739$. The solutions of the SP equation satisfy the relation $\cos\varphi_{1,2} = [-1 \pm \sqrt{1 - 4\xi(a_0 - \xi/2)}]/(2\xi)$. For $\xi \gtrsim 0.954$, both signs are acceptable with respect to the constraint $-1 \le \cos\varphi \le 1$, so that we have four solutions ($\varphi_{1,2}$ and $2\pi - \varphi_{1,2}$). On the other hand, for $\xi \lesssim 0.524$ only the plus sign is permitted and there are only two real solutions (φ_1 and $2\pi - \varphi_1$).

The partial contributions of the SP solutions, together with their coherent sum and the result obtained using the numerical integration, are presented in Fig. 1 for $\xi = 0.4$ and 2. For $\xi = 0.4$ there are two SP solutions ($\eta = 1, 2$) for all values of the electron final energy. These solutions are symmetric with respect to $t = T/2$ and lead to the same partial contributions to the DCS. The interference between the contributions of these solutions produces slow and deep oscillations of the electron spectrum. On the other hand, for $\xi = 2$ there are four SP solutions ($\eta = 1, 2, 3, 4$) for all values of E_f. The resulting spectrum exhibits rapid oscillations caused by the interference of the contributions of all four partial amplitudes. Analytical solutions can also be found for $\phi = \pi$. For other values of the relative phase ϕ and for a general multicolor field with arbitrary values of the parameters the information regarding the number of SP solutions cannot be extracted analytically. In order to show how catastrophe theory can help to characterize these solutions, we consider the ω–2ω field for which the fold, cusp, and swallowtail catastrophes appear, and the ω–2ω–3ω trichromatic field for which high-codimensional catastrophes can be found. For energies near and beyond the cutoffs (denoted by $L = 45$ and $L = 128$ in Fig. 1) the SP method fails and one should use the uniform approximation [63]. The energies beyond the cutoff are classically forbidden and the saddle-point solutions of the equation $S'_L(t) = 0$ are complex-valued. We will not consider this case in the present paper.

Folds, cusp, swallowtail, and wigwam catastrophes for LAS

For the ω–2ω field the number of real solutions depends on the relative phase ϕ, the field amplitude ratio ξ, and an effective parameter a_0. In this case, the parametrized action $\mathcal{S}(t;\mathcal{C})$ can be written as $\mathcal{S}(\varphi;\xi,\phi,a_0) = L[a_0\varphi + \sin\varphi + \xi\sin(2\varphi+\phi)/4]/a_0$, where instead of the scattering time t we used the variable $\varphi = \omega t$, and we explicitly

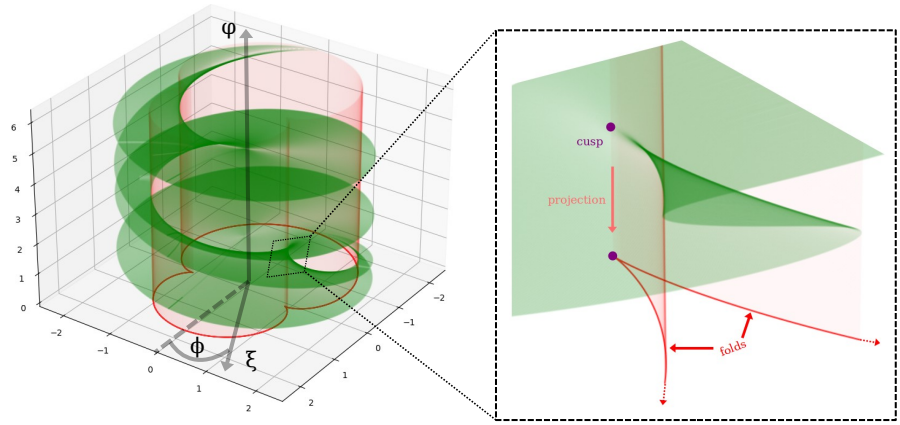

Fig. 2 Catastrophe surface.
The catastrophe surface $\mathcal{S}'(\varphi;\xi,\phi,a_0)=0$ (in green) for the fixed value of the parameter $a_0=0.1$, and for our ω–2ω field. Inset illustrates cusp (purple circle) and folds (red curves) obtained as projections onto the control parameter space [(ξ,ϕ) plane].

denoted the control parameters. In the language of catastrophe theory [28], the surface of solutions of equation $\mathcal{S}'=0$ contains catastrophes of maximum control dimension three and corank one and the possible structurally stable catastrophes are fold, cusp, and swallowtail. The parameter dependence of the surface of solutions can be visualized by plotting the positions of these catastrophes in the parameter space. For a fixed value of the parameter a_0, equation $\mathcal{S}'=0$ represents the catastrophe surface in the three-dimensional space $(x,y,z)=(\xi\cos\phi,\xi\sin\phi,\varphi)$. Projection of the degenerate critical points of this surface onto the (x,y) plane shows two fold strata which meet at the cusp point (see Fig. 2). For a fixed value of the control parameter a_0 we eliminate the variable φ from the system of equations $\mathcal{S}'=0$ and $\mathcal{S}''=0$ and present the solutions for the parameters ξ and ϕ in polar coordinates. Repeating this for a set of values of a_0 we get three-dimensional figure in the $(\xi\cos\phi,\xi\sin\phi,a_0)$ space. This is shown in Fig. 3 which represents the bifurcation set for our ω–2ω field. The swallowtail catastrophe appears at the place where a pair of one-dimensional cusp strata meet and end. This is illustrated in Fig. 3 where we use clipping to extract the relevant part of the graph with the swallowtail.

In Fig. 4a)–d), for a range of values of the parameter a_0, we plot the points in the parameter space in polar coordinates (ξ,ϕ) for which $\mathcal{S}'=\mathcal{S}''=0$ (red curves correspond to the fold catastrophe; see Supplementary Note 1). For the values of ξ and ϕ for which the spikes appear the third derivative of the action is also zero [this

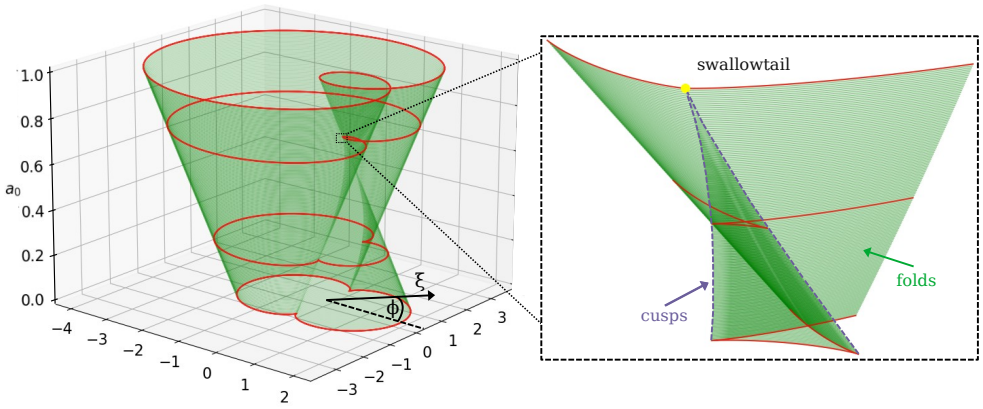

Fig. 3 Bifurcation set.
The bifurcation set for our ω–2ω field, presented as the green surface in the three-dimensional control parameter space. The intersections of this surface with the fixed-a_0 planes are denoted by the red lines. Inset illustrates swallowtail catastrophe.

is the cusp catastrophe; cf. Fig. 2 and the orange solid line in Fig. 4a)]. For every ϕ, moving along the line of increasing ξ, the number of real SP solutions changes by two whenever the red line is crossed. Also, the logarithm of the DCS in the (ξ, ϕ) polar plane is presented for a fixed value of the parameter a_0. The qualitative changes in the spectral pattern, such as the onset of the sharp modulations, the appearance of the new structures, or sudden variations in the contrast, occur exactly at the position of the red lines. The patterns visible in the DCS maps are in agreement with the patterns corresponding to the diffraction catastrophes shown in Fig. 1 of [67]. For the fold, the Airy-type oscillations appear, while for the cusp, the more complex three-trajectory interference domain is prominent.

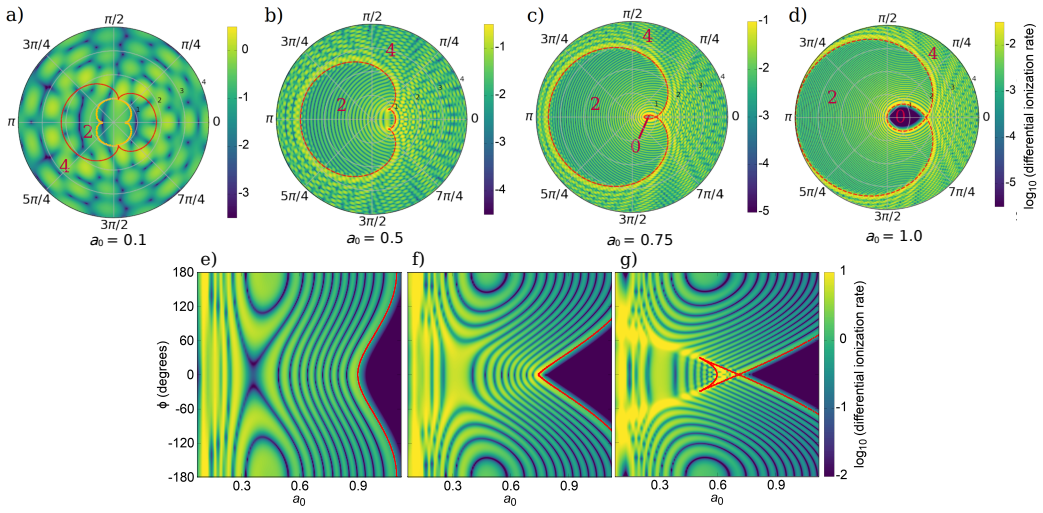

Fig. 4 Differential cross section and the bifurcation sets.
Logarithm of the DCS and the bifurcation sets (red lines) for our ω–2ω field. Panels a)–d): The results presented in the (ξ, ϕ) polar plane for fixed values of the parameter a_0 as indicated below the panels. The number of solutions is displayed in red. The orange solid line in a) denotes the points in the full parameter space for which $\mathcal{S}' = \mathcal{S}'' = \mathcal{S}''' = 0$, projected into the (ξ, ϕ) plane. Panels e)–g) show the results presented in the (a_0, ϕ) plane for fixed values of the parameter ξ: e) $\xi = 0.2$, f) $\xi = 0.5$, and g) $\xi = 0.8$.

To further illustrate how fixing one of the control parameters constrains and reshapes the bifurcation landscape, in Fig. 4e)–g) we present the differential cross section and the bifurcation sets for three fixed values of the field-amplitude ratio ξ. By scanning over a_0 and ϕ, while keeping ξ constant, we obtain the corresponding two-dimensional projections of the fold and cusp. For $\xi = 0.5$ [panel f)], the bifurcation pattern develops a swallowtail structure for $a_0 = 0.75$ and $\phi = 0°$, signalling the coalescence of four stationary points. This behavior is consistent with the caustic formation observed experimentally and theoretically in [38].

For a trichromatic ω–2ω–3ω field $E(t) = E_0[\sin(\omega t) + \xi \sin(2\omega t + \phi) + \rho \sin(3\omega t + \psi)]$, we have five control parameters ξ, ϕ, ρ, ψ, and a_0, which brings us beyond the Thom's catastrophes. A 3-dimensional slice of our catastrophe surface (and corresponding 2-dimensional slice of the bifurcation set) is illustrated in Fig. 5, for a set of parameters in the vicinity of the A_6 (wigwam) catastrophe point (see Supplementary Note 2). We are showing a fixed 3D cross-section of the catastrophe surface, such that the corresponding 2D cross-section of its bifurcation set resembles the characteristic cross-sectional bifurcation set of the wigwam catastrophe. The case of a trichromatic field is particularly interesting because a few-cycle pulse with a sine-square envelope can be presented by this type of the field [68].

For a general multicolor driving field, the number of control parameters grows rapidly with the number of field components, leading to various catastrophes, all of which remain of corank one. As the parameter space expands, higher codimension

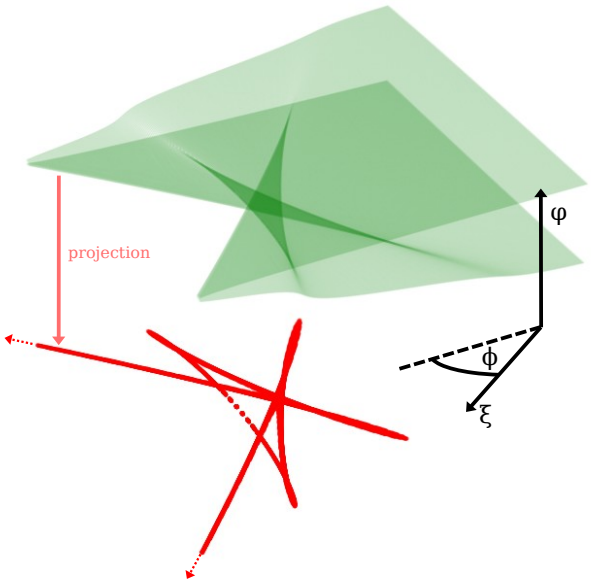

Fig. 5 Wigwam catastrophe.
Presentation of a section of A_6 (wigwam) catastrophe in the $(\xi\cos\phi, \xi\sin\phi, \varphi)$ space with fixed values of the control parameters $\rho = 0.2$, $\psi = 0$, and $a_0 = 2/3$, for the LAS process in our ω–2ω–3ω field. The projection of critical points in the polar (ξ, ϕ) plane is depicted by the red curve. The A_6 catastrophe appears at the point $(\xi, \phi) = (0.8, 0)$.

singularities emerge, giving rise to increasingly complex bifurcation sets and spectral transitions. This highlights that multicolor fields provide a flexible platform where essentially all cuspoid (A_n) catastrophes can, in principle, be realized.

Conclusions

In this work, we have presented the laser-assisted scattering amplitude in the form of an integral over the scattering time, where the phase is a large laser-field-dependent action. This structure allows the application of asymptotic methods for integrals to express the scattering amplitude as a sum of partial contributions corresponding to stationary points. The interference between these partial amplitudes determines the shape of the differential cross-section. When only a few stationary points are relevant, the spectrum is smooth; as their number increases, the spectrum becomes highly oscillatory or even erratic.

For specific field configurations, the number of stationary points can be determined analytically. However, in more general cases, we have shown that catastrophe theory provides a systematic way to identify critical values of the control parameters where transitions between different spectral regimes occur, even without explicitly calculating the scattering amplitude. The classification of catastrophes also enables the appropriate selection of asymptotic methods, such as the stationary-phase method or

uniform approximations for two coalescing points and for higher-order catastrophe integrals, tailored to the structure of the problem.

The approach developed here introduces a framework for the analysis of laser-assisted scattering processes, based on the geometric and topological structures revealed by catastrophe theory. This methodology is not restricted to scattering but is sufficiently general to be extended to laser-induced processes, offering pathways for exploring critical behaviors in a wide range of strong-field phenomena. It provides not only predictive power regarding the number and type of contributing trajectories but also deeper insight into the physical mechanisms that govern these processes. For laser-induced processes, such as high-order harmonic generation, (high-order) above-threshold ionization, and non-sequential double (multiple) ionization, the presence of tunnelling forces all saddle points to be complex-valued. Furthermore, even for laser-assisted processes there are classically forbidden parameter regions where the complex saddle-point solutions have to be used. For example, in Fig. 1 beyond the cutoff energy the SP method fails and one has to use complex saddle-point solutions and the uniform approximation [63]. The catastrophe-theory formalism with complex-valued saddle points is more complicated and should also be applied to strong-field processes and its formulation remains an open problem.

Furthermore, the analysis of phase behavior near critical points is particularly important for the characterization of phenomena such as attosecond pulse generation [38], where caustic structures play a decisive role. The ability to systematically locate and classify critical points highlights the broader potential of catastrophe theory in strong-field physics and attoscience, offering a conceptually new perspective on the underlying dynamics of laser-assisted and laser-induced processes.

Acknowledgements
We gratefully acknowledge support by the Alexander von Humboldt Foundation.

Author contributions
D.H., T.R., and D.B.M. contributed equally to this work.

Competing interests
The authors declare no competing interests.

Data availability
The data are available from the authors upon request.

Code availability
The code that supports the findings of this study is available from the authors upon request.

References

[1] Mourou, G. Nobel Lecture: Extreme light physics and application. *Rev. Mod. Phys.* **91**, 030501 (2019).

[2] Strickland, D. Nobel Lecture: Generating high-intensity ultrashort optical pulses. *Rev. Mod. Phys.* **91**, 030502 (2019).

[3] Agostini, P. Nobel Lecture: Genesis and applications of attosecond pulse trains. *Rev. Mod. Phys.* **96**, 030501 (2024).

[4] Krausz, F. Nobel Lecture: Sub-atomic motions. *Rev. Mod. Phys.* **96**, 030502 (2024).

[5] L'Huillier, A. Nobel Lecture: The route to attosecond pulses. *Rev. Mod. Phys.* **96**, 030503 (2024).

[6] Milošević, D. B. & Ehlotzky, F. Scattering and reaction processes in powerful laser fields. *Adv. At. Mol. Opt. Phys.* **49**, 373–532 (2003).

[7] Joachain, C. J., Kylstra, N. J. & Potvliege, R. M. *Atoms in Intense Laser Fields* (Cambridge University Press, 2011).

[8] Weingartshofer, A., Holmes, J. K., Caudle, G., Clarke, E. M. & Krüger, H. Direct Observation of Multiphoton Processes in Laser-Induced Free-Free Transitions. *Phys. Rev. Lett.* **39**, 269–272 (1977).

[9] Ehlotzky, F., Jaroń, A. & Kamińsky, J. Z. Electron-atom collisions in a laser field. *Phys. Rep.* **297**, 63–153 (1998).

[10] Milošević, D. B. & Ehlotzky, F. X-ray-atom scattering in the presence of a laser field. *Phys. Rev. A* **58**, 2319–2326 (1998).

[11] Milošević, D. B. & Starace, A. F. Static-Electric-Field-Induced, High-Energy Plateau for Scattered X-Ray Photons in Laser-Assisted, X-Ray–Atom Scattering. *Phys. Rev. Lett.* **81**, 5097–6000 (1998).

[12] Jaroń, A., Kamiński, J. Z. & Ehlotzky, F. Stimulated radiative recombination and x-ray generation. *Phys. Rev. A* **61**, 023404 (2000).

[13] Kuchiev, M. Y. & Ostrovsky, V. N. Multiphoton radiative recombination of electron assisted by a laser field. *Phys. Rev. A* **61**, 033414 (2000).

[14] Becker, W., Grasbon, F., Kopold, R., Milošević, D. B., Paulus, G. G. & Walther, H. Above-threshold ionization: From classical features to quantum effects. *Adv. At. Mol. Opt. Phys.* **48**, 35–98 (2002).

[15] Lein, M. Molecular imaging using recolliding electrons. *J. Phys. B* **40**, R135–R173 (2007).

[16] Krausz, F. & Ivanov, M. Attosecond physics. *Rev. Mod. Phys.* **81**, 163–234 (2009).

[17] Lin, C. D., Le, A.-T., Chen, Z., Morishita, T. & Lucchese, R. Strong-field rescattering physics—self-imaging of a molecule by its own electrons. *J. Phys. B* **43**, 122001 (2010).

[18] Kohler, M. C., Pfeifer, T., Hatsagortsyan, K. Z. & Keitel, C. H. Frontiers of atomic high-harmonic generation. *Adv. At. Mol. Opt. Phys.* **61**, 159–208 (2012).

[19] Popruzhenko, S. V. Keldysh theory of strong field ionization: history, applications, difficulties and perspectives. *J. Phys. B* **47**, 204001 (2014).

[20] Wolter, B. et al. Strong-Field Physics with Mid-IR Fields. *Phys. Rev. X* **5**, 021034 (2015).

[21] Figueira de Morrison Faria, C. & Maxwell, A. S. It is all about phases: ultrafast holographic photoelectron imaging. *Rep. Prog. Phys.* **83**, 034401 (2020).

[22] Bauer, D. (ed.), *Computational strong-field quantum dynamics: Intense Light-Matter Interactions* (De Gruyter Textbook, Berlin, 2016).

[23] Bunkin, F. V. & Fedorov, M. V. Bremsstrahlung in a strong radiation field. *Sov. Phys. JETP* **22**, 844–847 (1966) [*Zh. Éksp. Teor. Fiz.* **49**, 1215–1221 (1965)].

[24] Agostini, P., Fabre, F., Mainfray, G., Petite, G. & Rahman, N. K. Free-Free Transitions Following Six-Photon Ionization of Xenon Atoms. *Phys. Rev. Lett.* **42**, 1127–1130 (1979).

[25] Ferray, M., L'Huillier, A., Li, X. F., Lompre, L. A., Mainfray, G. & Manus, C. Multiple-harmonic conversion of 1064-nm radiation in rare gases. *J. Phys. B* **21**, L31–L35 (1988).

[26] Mason, N. J. Laser-assisted electron-atom collisions. *Rep. Prog. Phys.* **56**, 1275–1346 (1993).

[27] Kanya, R. & Yamanouchi, K. Femtosecond laser-assisted electron scattering for ultrafast dynamics of atoms and molecules. *Atoms* **7**, 85 (2019).

[28] Thom, R. *Structural stability and morphogenesis: An outline of a general theory of models* (W. A. Benjamin, Inc., Reading, 1975) [English translation of: Thom, R. *Stabilité Structurelle et Morphogénèse: Essai d'une théorie générale des modèles* (InterEditions, Paris, 1972)].

[29] Zeeman, E. C. Catastrophe theory. *Sci. Am.* **234**, 65–83 (1976).

[30] Arnold, V. I. *Catastrophe Theory* (Springer Science & Business Media, 2003).

[31] Arnold, V. I. Critical points of smooth functions and their normal forms. *Russ. Math. Surv.* **30**, 1–75 (1975) [*Uspekhi Mat. Nauk* **30**, 3–65 (1975)].

[32] Berry, M. V. Waves and Thom's theorem. *Adv. Phys.* **25**, 1–26 (1976).

[33] Berry, M. V. & Upstill, C. IV Catastrophe Optics: Morphologies of Caustics and Their Diffraction Patterns. *Prog. Opt.* **18**, 257–346 (1980).

[34] Stewart, I. Catastrophe theory in physics. *Rep. Prog. Phys.* **45**, 185–221 (1982).

[35] Castrigiano, D. P. L. & Hayes, S. A. *Catastrophe Theory*, 2nd ed. (Taylor & Francis Group LLC, Boca Raton, 2004).

[36] Montaldi, J. *Singularities, Bifurcations and Catastrophes* (Cambridge University Press, 2021).

[37] Milošević, D. B. & Becker, W. Role of long quantum orbits in high-order harmonic generation, *Phys. Rev. A* **66**, 063417 (2002).

[38] Raz, O., Pedatzur, O., Bruner, B. D. & Dudovich, N. Spectral caustics in attosecond science. *Nat. Photonics* **6**, 170–173 (2012).

[39] Faccialà, D. et al. Probe of Multielectron Dynamics in Xenon by Caustics in High-Order Harmonic Generation. *Phys. Rev. Lett.* **117**, 093902 (2016).

[40] Birulia, V. A. & Strelkov, V. V. Spectral caustic in two-color high-order harmonic generation: Role of Coulomb effects. *Phys. Rev. A* **99**, 043413 (2019).

[41] Pisanty, E., Ciappina, M. F. & Lewenstein, M. The imaginary part of the high-harmonic cutoff. *J. Phys. Photonics* **2**, 034013 (2020).

[42] Uzan, A. J. et al. Attosecond spectral singularities in solid-state high-harmonic generation. *Nat. Photonics* **14**, 183–187 (2020).

[43] Chen, J., Xia, Q. & Fu, L. Spectral caustics of high-order harmonics in one-dimensional periodic crystals. *Opt. Lett.* **46**, 2248–2251 (2021).

[44] Figueira de Morisson Faria, C., Schomerus, H. & Becker, W. High-order above-threshold ionization: The uniform approximation and the effect of the binding potential. *Phys. Rev. A* **66**, 043413 (2002).

[45] Milošević, D. B., Hasović, E., Busuladžić, M., Gazibegović-Busuladžić, A. & Becker, W. Intensity-dependent enhancements in high-order above-threshold ionization. *Phys. Rev. A* **76**, 053410 (2007).

[46] Kelvich, S. A., Becker, W. & Goreslavski, S. P. Coulomb focusing and defocusing in above-threshold-ionization spectra produced by strong mid-IR laser pulses. *Phys. Rev. A* **93**, 033411 (2016).

[47] Kelvich, S. A., Becker, W. & Goreslavski, S. P. Caustics and catastrophes in above-threshold ionization. *Phys. Rev. A* **96**, 023427 (2017).

[48] Xia, Q. Z., Tao, J. F., Cai, J., Fu, L. B. & Liu, J. Quantum Interference of Glory Rescattering in Strong-Field Atomic Ionization. *Phys. Rev. Lett.* **121**, 143201 (2018).

[49] López, S. D. & Arbó, D. G. Holographic interference in atomic photoionization from a semiclassical standpoint. *Phys. Rev. A* **100**, 023419 (2019).

[50] Morishita, T. & Tolstikhin, O. I. Adiabatic theory of strong-field photoelectron momentum distributions near a backward rescattering caustic. *Phys. Rev. A* **96**, 053416 (2017).

[51] Flegel, A. V. et al. Analytic description of the above-threshold detachment in the adiabatic limit. *Phys. Rev. A* **102**, 063119 (2020).

[52] Mizuno, T. et al. Comparative study of photoelectron momentum distributions from Kr and CO_2 near a backward rescattering caustic by carrier-envelope-phase mapping. *Phys. Rev. A* **107**, 033101 (2023).

[53] Rook, T., Rodriguez, L. C. & Figueira de Morisson Faria, C. Influence of catastrophes and hidden dynamical symmetries on ultrafast backscattered photoelectrons. *Phys. Rev. Res.* **6**, 023329 (2024).

[54] Seipt, D., Surzhykov, A., Fritzsche, S. & Kämpfer, B. Caustic structures in x-ray Compton scattering off electrons driven by a short intense laser pulse. *New J. Phys.* **18**, 023044 (2016).

[55] Kharin, V. Yu., Seipt, D. & Rykovanov, S. G. Higher-Dimensional Caustics in Nonlinear Compton Scattering. *Phys. Rev. Lett.* **120**, 044802 (2018).

[56] Milošević, D. B. Potential scattering in a strong multicolour laser field. *J. Phys. B* **29**, 875–893 (1996).

[57] Feynman, R. P. & Hibbs, A. R. *Quantum Mechanics and Path Integrals* (McGraw-Hill, New York, 1965).

[58] Salières, P. et al. Feynman's Path-Integral Approach for Intense-Laser–Atom Interactions. *Science* **292**, 902–905 (2001).

[59] Milošević, D. B., Jašarević, A. S., Habibović, D., Hasović, E., Čerkić, A., & Becker, W. Asymptotic methods applied to integrals occurring in strong-laser-field processes. *J. Phys. A* **57**, 393001 (2024).

[60] Wong, R. *Asymptotic Approximations of Integrals* (Academic, Boston, 1989).

[61] Borovikov, V. A. *Uniform Stationary Phase Method* (The Institution of Electrical Engineers, London, 1994).

[62] Čerkić, A. & Milošević, D. B. Plateau structures in potential scattering in a strong laser field. *Phys. Rev. A* **70**, 053402 (2004).

[63] Čerkić, A. & Milošević, D. B. Interferences of real trajectories and the emergence of quantum features in electron-atom scattering in a strong laser field. *Phys. Rev. A* **73**, 033413 (2006).

[64] Delone, N. B., Manakov, N. L. & Fainstein, A. G. Ionization of atoms by a low-frequency field and an optical-frequency field. *Sov. Phys. JETP* **59**, 529–533 (1984) [*Zh. Eksp. Teor. Fiz.* **86**, 906–914 (1984)].

[65] Manakov, N. L., Ovsiannikov, V. D. & Rapoport, L. P. Atoms in a laser field. *Phys. Rep.* **141**, 319–433 (1986).

[66] Jašarević, A., Hasović, E., Kopold, R., Becker, W. & Milošević, D. B. Application of the saddle-point method to strong-laser-field ionization. *J. Phys. A* **53**, 125201 (2020).

[67] Berry, M. V. & Klein, S. Colored diffraction catastrophes. *Proc. Natl. Acad. Sci. USA* **93**, 2614–2619 (1996).

[68] Čerkić, A. & Milošević, D. B. Few-cycle laser-pulse-assisted electron-atom potential scattering. *Phys. Rev. A* **87**, 033417 (2013).

Caption of Figure 1:
Differential cross section for laser-assisted scattering.
The partial contributions of the SP solutions to the DCS for electron scattering on the He atom in the presence of the ω–2ω field as a function of the number of exchanged photons L. The ratio of the electric-field amplitudes is: a) $\xi = 0.4$ and b) $\xi = 2$, as denoted in the panels. The laser intensity, relative phase, and wavelength are $E_0^2 = 3 \times 10^{14}$ W cm^{-2}, $\phi = 0$, and 1000 nm, respectively. The initial electron kinetic energy is 0.5 a.u. and the electron momenta are in the polarization direction. We also present the coherent sum of the partial contributions (blue line, circles) and the exact result (black solid line). The insets show the SP solutions.

Caption of Figure 2:
Catastrophe surface.
The catastrophe surface $\mathcal{S}'(\varphi; \xi, \phi, a_0) = 0$ (in green) for the fixed value of the parameter $a_0 = 0.1$, and for our ω–2ω field. Inset illustrates cusp (purple circle) and folds (red curves) obtained as projections onto the control parameter space [(ξ, ϕ) plane].

Caption of Figure 3:
Bifurcation set.
The bifurcation set for our ω–2ω field, presented as the green surface in the three-dimensional control parameter space. The intersections of this surBface with the fixed-a_0 planes are denoted by the red lines. Inset illustrates swallowtail catastrophe.

Caption of Figure 4:
Differential cross section and the bifurcation sets.
Logarithm of the DCS and the bifurcation sets (red lines) for our ω–2ω field. Panels a)–d): The results presented in the (ξ, ϕ) polar plane for fixed values of the parameter a_0 as indicated below the panels. The number of solutions is displayed in red. The orange solid line in a) denotes the points in the full parameter space for which $\mathcal{S}' = \mathcal{S}'' = \mathcal{S}''' = 0$, projected into the (ξ, ϕ) plane. Panels e)–g) show the results presented in the (a_0, ϕ) plane for fixed values of the parameter ξ: e) $\xi = 0.2$, f) $\xi = 0.5$, and g) $\xi = 0.8$.

Caption of Figure 5:
Wigwam catastrophe.
Presentation of a section of A_6 (wigwam) catastrophe in the $(\xi \cos\phi, \xi \sin\phi, \varphi)$ space with fixed values of the control parameters $\rho = 0.2$, $\psi = 0$, and $a_0 = 2/3$, for the LAS process in our ω–2ω–3ω field. The projection of critical points in the polar (ξ, ϕ) plane is depicted by the red curve. The A_6 catastrophe appears at the point $(\xi, \phi) = (0.8, 0)$.